Band inversion induced large-gap quantum spin Hall states in III-Bi-monolayer/SiO_2

Yunyouyou Xia,[1,2,*] Suhua Jin,[1,*] Jiayu Hu,[1] Ralph Claessen,[3,4] Werner Hanke,[5,4] Ronny Thomale,[5,4] and Gang Li[1,2,†]

[1]*School of Physical Science and Technology, ShanghaiTech University, Shanghai 201210, China*

[2]*ShanghaiTech Laboratory for Topological Physics, ShanghaiTech University, Shanghai 201210, China*

[3]*Physikalisches Institut, Universität Würzburg, D-97074 Würzburg, Germany*

[4]*Würzburg-Dresden Cluster of Excellence ct.qmat, Universität Würzburg, D-97074 Würzburg, Germany*

[5]*Institut für Theoretische Physik und Astrophysik, Universität Würzburg, D-97074 Würzburg, Germany*

(Received 27 February 2022; accepted 6 September 2022; published 11 October 2022)

We extend the p_x-p_y large-gap scenario to the band inversion systems and exemplify the mechanism with a family of III-Bi honeycomb monolayers on SiO_2, which can be the next generation of large-gap quantum spin Hall (QSH) systems. First, it suggests a topological gap of the same order as the current record kept of bismuthene/SiC(0001). Second, the band inversion mechanism in which these QSH insulators originate is qualitatively distinct from the Kane-Mele paradigm. Our work demonstrates that the p_x-p_y scenario can be utilized to promote large-gap QSH states with both Kane-Mele and band inversion mechanisms, providing an efficient building principle for future topological device construction.

DOI: 10.1103/PhysRevB.106.165203

I. INTRODUCTION

Quantum spin Hall (QSH) insulators are considered as one of the key ingredients for a new era of spintronics devices utilizing dissipationless edge spin currents. Yet, after initial suggestions in graphene [1,2] and experimental observation in HgTe quantum wells [3,4], most proposed QSH systems evade further device applications due to insufficient topological gaps or poor chemical stability. This has led to tremendous material research activity in obtaining experimentally feasible high-temperature QSH systems. Throughout the principal lines of proposals for a QSH setup, the topological bulk gaps are closely associated with the spin-orbit coupling (SOC) strength. Hence, within the bounds of graphene-type systems, elemental honeycomb sheets containing heavy Xenes (X denotes element, e.g., silicene [5], germanene [5], stanene [6], and bismuthene [7–9]) were predicted to possess sizable topological bulk gaps. Substantial progress was achieved in the monolayer-substrate heterostructure bismuthene on SiC(0001) [10,11]. It exhibits the so far largest QSH gap (∼800 meV) measured in the experiment. From the viewpoint of the Kane-Mele paradigm, the Bi/SiC monolayer/substrate heterostructure offers a "best of two worlds" scenario: the substrate not only stabilizes the QSH insulator but also enlarges the topological gap via orbital filtering.

The successful fabrication of bismuthene/SiC(0001) is significantly facilitated by improvements in preparing a smooth and defect-free SiC(0001) surface with hydrogen termination [12], which is a highly challenging task and is critical to the topological nature of the heterostructure. The surface of the substrate needs to be smooth enough to a large extent to host the flat bismuthene monolayer. At the same time, the bismuth honeycomb needs to selectively bond with the underlying silicon which arranges in a triangular form. Consequently, not every silicon atom at the surface of SiC(0001) will be saturated, and there is one silicon remaining in each hexagon to be hydrogenated.

The QSH states in bismuthene/SiC(0001) enjoy the presence of substrate as it removes the p_z orbital and, at the same time, stables the bismuthene monolayer. However, QSH Xene heterostructures also exhibit further complexity through broken inversion symmetry, which, in particular around the K point, leads to sizable Rashba splitting. Such a Rashba splitting does not cooperate with the topology, but rather reduces the band gap. In bismuthene/SiC(0001), the conduction band minimum lies at Γ rather than K. The resulting indirect gap, together with the sizable Rashba splitting at K, results in a global gap smaller than what $p_{x/y}$ could intrinsically support. Overcoming the aforementioned indirect gap and Rashba limitations hence is the central guiding principle to improve the bismuthene paradigm of the p-orbital hexagonal QSH heterostructure. Recently, the material search was extended to alloy-type inversion-asymmetric III-V binary monolayers [13,14]. Among them, the freestanding buckled III-Bi monolayer was predicted to host QSH states with gaps up to around 560 meV [13]. To simulate the bonding effects of substrates, hydrogenated [15–19], halogenated [16,18,20–22], and molecule-functionalized [23–26] III-V films were studied, and in part are claimed to preserve both stability and nontrivial edge states. Moreover, the possible synthesis of III-V monolayers on Si(111) [15,27–29], h-BN [20,23–25], and SrTe(111) [26] substrates has been predicted.

In this paper, we examine the possibility of boosting a large topological gap in band inversion type systems with the p_x-p_y mechanism and propose III-V honeycomb monolayers on SiO_2 substrate to be a new platform for large-gap QSH states that are ready for experiments to verify. Most importantly, we find that this platform could strike an optimal

*These authors contributed equally to this work.

†ligang@shanghaitech.edu.cn

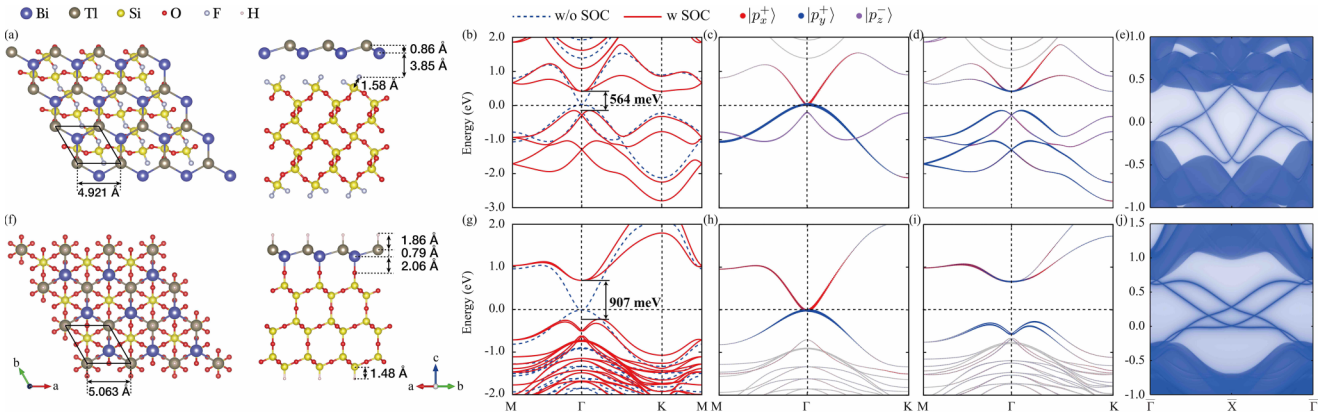

FIG. 1. III-V-monolayer/SiO_2. (a) Crystalline structures of TlBi/α-SiO_2 in top and side view. A similar but enlarged plot can be found in the Supplemental Material [30]. (b) Electronic structures of TlBi/α-SiO_2. (c), (d) Projection of Bloch bands on bonding/antibonding states without (c) and with (d) the SOC of TlBi/α-SiO_2. (e) The zigzag edge states of TlBi/α-SiO_2. (f)–(j) The same plot for TlBi/β-SiO_2.

compromise between a large topological gap and experimental feasibility. Regarding experimental feasibility, the two silica polymorphs support the III-V monolayer in different ways and thus partially relax the critical bonding requirement witnessed in bismuthene/SiC(0001). Furthermore, they realize a band inversion type QSH phase, which is different from the Kane-Mele type mechanism implemented in bismuthene/SiC(0001), making the p_x-p_y scenario a flexible and promising design principle for large-gap QSH states.

II. III-V-MONOLAYER/SiO_2

We first briefly discuss the material setup and, then, devote our main effort to discussing the effect of the p_z orbital in these systems. There are two ways to overlay thin films on substrates, i.e., via van der Waals interactions and via chemical bonding. The latter may strongly modify the low-energy electronic structure of the thin films, which can either devastate the topological nature or enhance the nontrivial gap. The second scenario was textbook-likely demonstrated in the bismuthene/SiC work.

Here, we propose two silica polymorphs as plausible substrates for III-V honeycomb monolayers, which are widely used traditional substrates taking advantage of excellent insulation, chemical stability, and compatibility with silicon. Specifically, we suggest synthesizing III-V films on α-quartz (denoted as α-SiO_2) and β-tridymite (denoted as β-SiO_2) silicon dioxides. Their experimentally determined lattice constant are 4.921 Å [37] and 5.063 Å [38], respectively. The equilibrium lattice constants of the three paradigm III-V films studied in this work are 4.805 Å (InBi), 4.928 Å (TlBi) [13], and 4.81 Å (TlSb) [14], rendering strain within a range of -0.14% to 5.37%, which are fairly reasonable values in experiments. All six monolayer-substrate systems support room-temperature QSH states with gaps over 200 meV. With α-SiO_2, the substrate is inert and interacts with III-V monolayers through the van der Waals force, retaining a topological gap of 564 meV in TlBi, while with β-SiO_2, the p_z orbital of the III-V film is bonded to the substrate, rendering a gap up to 907 meV.

In the geometry with α-SiO_2 [Fig. 1(a)], the III-V film is constructed on the (001) plane of the substrate with the center of the hexagonal cell above the top silicon atoms. The dangling bonds of the substrate are saturated by fluorination, in the simulation of an experimentally passivated/terminated surface. Hence the III-V film does not directly bond with α-SiO_2 but rather interacts weakly through van der Waals forces. The substrate hardly affects the electronic structure of III-V, leaving the bands around the Fermi level similar to the freestanding III-V films [Fig. 1(b)]. By inspecting orbital characteristics [Figs. 1(c) and 1(d)], we show that the band degeneracy of the bonding/antibonding orbitals $|p_x^+\rangle$ and $|p_y^+\rangle$ is lifted by the SOC, inducing an indirect gap of 564 meV. The conduction and valance bands show detectable Rashba splitting, primarily induced by the lower $|p_z^-\rangle$ state, as will be explained in the latter model discussion.

In the geometry with β-SiO_2 [Fig. 1(f)], the III-V film is constructed on the (001) plane of SiO_2 with group-V atoms above the top oxygen atoms. The strong bonding significantly alters the band structure of the film via an orbital filtering effect. The $|p_z^-\rangle$ orbitals of the III-V monolayer are saturated by bonding to the oxygen dangling bonds, and the bands around the Fermi level merely come from $|p_x^+\rangle$ and $|p_y^+\rangle$ [Figs. 1(h) and 1(i)]. They do not display any sizable Rashba splitting. As compared to III-V-monolayer/α-SiO_2, the SOC-induced gap in III-V-monolayer/β-SiO_2 is significantly enhanced to 907 meV in TlBi, larger than bismuthene/SiC gap estimated by the same level of DFT approximation.

We further verify that the nontrivial bulk bands in both systems herald the presence of edge modes inside the energy gap and the Wilson loop (Fig. SI-4 of the Supplemental Material [30]). As attested in Figs. 1(e) and 1(j), the III-V films combined with the two substrates host topologically nontrivial QSH edge states. The flexibility in overlaying topological monolayers and the relatively easy preparation of a large-scale smooth surface of SiO_2 reduce the challenge in experimental fabrication and may provide III-V-monolayer/SiO_2 as a second prototype large-gap QSH system.

III. TOPOLOGICAL ORIGIN AND ROLE OF p_z

After confirming the topological nature and the enhanced bulk gap, we further address the topological origins of III-V-monolayer/SiO_2 and compare it to

bismuthene/SiC(0001). In III-V honeycomb films, in addition to the p_x and p_y orbitals actively participating in bismuthene/SiC, the p_z orbital contributes equally. Thus, we use all three p orbitals to construct a tight-binding model using Slater-Koster integrals [39]. For simplicity, we first include up to the nearest neighbor hopping terms. They are sufficient for correctly interpreting the low-energy electronic structure and the associated topology. Longer-range hopping terms will further improve the quality of the model, but they are not crucial for the following analysis (see the Supplemental Material [30] for more information).

Without the SOC, the Hamiltonian is a 6×6 matrix spanning on the orbital and site basis $(p_x, p_y, p_z) \otimes (A, B)$. The III-V films are buckled and there exists a small but non-negligible hopping along the perpendicular direction between the A-B sublattices on both α- and β-SiO_2 substrates, which is absent in bismuthene. The buckling structure is also consistent with the presence of the p_z orbital in the low-energy electronic structure. We note that such a 6×6 matrix contains redundant information. The low-energy electronic structures of the III-V honeycomb film on SiO_2 are mainly dominated by three bands, with the other three eigenvalues of the 6×6 Hamiltonian lying at higher energy. The p orbitals from A and B sites form bonding/antibonding states $p^+_{\alpha,\sigma}/p^-_{\alpha,\sigma}$, where α denotes the three components of the p orbital, and σ denotes the spin. The local C_{3v} symmetry requires $p^+_{x,\sigma}$ $(p^-_{x,\sigma})$ and $p^+_{y,\sigma}$ $(p^-_{y,\sigma})$ to be degenerate at the Γ point in the spinless case. According to the DFT guidance, we choose a group of parameters setting the $p^+_{x,\sigma}/p^+_{y,\sigma}$ degeneracy at the Fermi level and the p^-_z band lower in energy. The three low-energy bands are shown in the first column of Fig. 2 as the red dashed line.

Next, we include the atomic SOC $\lambda \boldsymbol{L} \cdot \boldsymbol{S}$ contribution to building up a relativistic analysis. The atomic SOC acting on three p orbitals links $p_{x,\sigma}$ and $p_{y,\sigma}$ with $L_z S_z$, $p_{x/y,\sigma}$, and $p_{z,-\sigma}$ with $L^{\pm}$. The former term is the dominant trigger of the topological gap between $p_{x/y,\sigma}$, and the latter one induces the Rashba splitting. In bismuthene/SiC(0001), the Rashba splitting of bands at K is solely due to the presence of the SiC substrate. In III-V-monolayer/SiO_2, the presence of the p_z orbital provides a new source of band Rashba splitting. The bands of the 12×12 relativistic model are shown as the blue solid line in Fig. 2(a), qualitatively resembling the case of III-V-monolayer/α-SiO_2 [Fig. 1(b)]. By constructing a nanoribbon, we find extra states connecting the conduction and valence bands inside the bulk gap [Fig. 2(c)], evidencing the hallmark of topological QSH edge states. In addition, the bands in Fig. 2(a) manifest clear Rashba splitting since the nonequivalent energy levels of the two III- and V-group elements break inversion symmetry even without the substrate.

After having convincingly shown that the tight-binding model captures all the essential features, we exploit the model to resolve contributing factors of the above SOC-induced topological gaps. We first dissemble the $\sigma\sigma$ and $\sigma\pi$ SOC contributions to examine their effects. By retaining $\langle p_{x,\sigma}|\boldsymbol{L} \cdot \boldsymbol{S}|p_{y,\sigma}\rangle$ but switching off $\langle p_{x/y,\sigma}|\boldsymbol{L} \cdot \boldsymbol{S}|p_{z,\sigma}\rangle$, we obtain a model conserving S_z. The band structure displays a band gap [the solid blue lines in Fig. 2(d)] triggered by the SOC between $p_{x/y}$ as in the case of bismuthene/SiC. Moreover, the Rashba band splitting is significantly weakened, which shifts up the valence band maximum. In consequence, the indirect topological gap is increased by an energy scale comparable to the Rashba splitting [comparing the solid blue lines and dashed red lines in Fig. 2(d)]. This indicates that, although it lies completely below the valence bands, the presence of the p_z orbital in III-V-monolayer/SiO_2 inevitably reduces the topological gap through the SOC with low-energy $p_{x/y}$ orbitals.

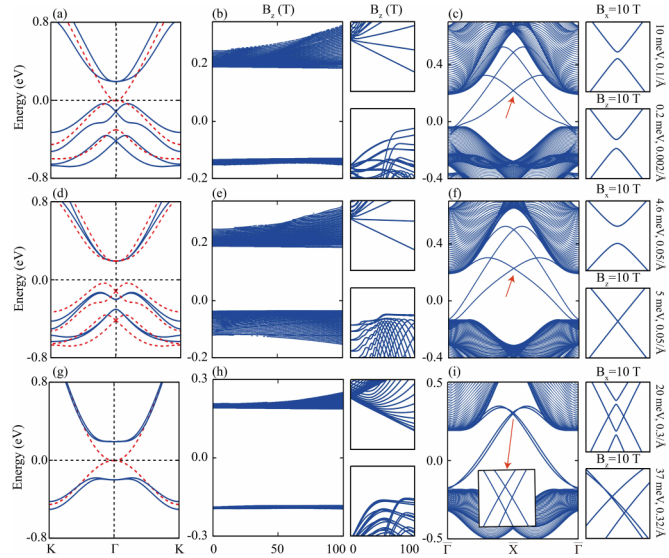

FIG. 2. Model Hamiltonian. (a) Spinless (dashed red line) and spinful (solid blue line) band structures with the basis p. (b) Landau levels as a function of a perpendicular magnetic field, with two zoomed-in plots on the right showing the conduction band bottom and valence band top evolution in an energy range of 10 meV. (c) Zigzag edge states are calculated from a nanoribbon with bulk bands as (a). (d) Comparison of spinful band structure (dashed red line) and band structure with vanishing $\langle p_{x/y,\sigma}|\boldsymbol{L} \cdot \boldsymbol{S}|p_{z,\sigma}\rangle$ (solid blue line). (e), (f) The same as (b), (c), but with vanishing $\langle p_{x/y,\sigma}|\boldsymbol{L} \cdot \boldsymbol{S}|p_{z,\sigma}\rangle$. (g)–(i) The same as (a)–(c), but with the basis $p_{x,y}$. The six zoomed-in plots on the right-hand side correspond to the edge Dirac points denoted by the red arrows in (c), (f), and (i) under magnetic fields $B_x = 10$ T ($B_z = 10$ T). They are gapped as long as p_z orbital is active. The energy and momentum ranges of these subplots are shown on the right of each.

The negative effect of p_z can be eliminated if the orbit is bonded. Removing $h^{ij}_{\alpha z}$ from the Hamiltonian matrix we reduce the model to 4×4 (8×8) in the basis of $(p_x, p_y) \otimes (A, B)$ for the spinless (spinful) case. The band structures and corresponding edge states with the same parameters as in Figs. 2(a) and 2(c) are shown in Figs. 2(g) and 2(i). Directly corresponding to III-V-monolayer/β-SiO_2, the SOC-induced topological gap is substantially magnified in the absence of p_z. This may accomplish another improvement over bismuthene/SiC. In both III-V-monolayer/β-SiO_2 and bismuthene/SiC, the low-energy physics is controlled by $p_{x/y}$ orbitals. They both show sizable band splitting, derived from either the inequivalent sublattices or the substrates. However, the band splitting is stronger at K and weaker at Γ in both systems. As a result, the gap size of III-V-monolayer/β-SiO_2 is hardly affected by the Rashba splitting. In this respect, for QSH states promoted by $p_{x/y}$ orbitals on honeycomb lattices, the largest topological gap can be potentially realized

by the mechanism of band inversion at Γ. This also explains why TlBi/β-SiO_2 harbors an even larger QSH gap than bismuthene/SiC does when Tl has a lower atomic number than Bi.

IV. MAGNETIC RESPONSE

After understanding the role of p_z on the topological gap size, next we examine its role in the magnetic response. In a band inversion type QSH system, the robustness of the nontrivial topology is controlled by the gap size at Γ instead of the indirect gap [40,41]. Thus, despite the small global gap, the quantized conductance inherent from the QSH states in an InAs/GaSb quantum well persists in a large magnetic field in the experiment, indicating that the breaking of time-reversal symmetry does not lead to an immediate trivialization of the system. In III-V-monolayer/SiO_2, the inverted band gap at Γ is much more pronounced, which is expected to promise a significant stabilization of the QSH states against the external magnetic field. Furthermore, as long as S_z is conserved, the topological edge states remain robust under a perpendicular magnetic field. However, inversion symmetry breaking will mix the p_z orbital with $p_{x/y}$ orbitals through SOC, breaking S_z conservation. Consequently, the topological edge states may become no longer stable. It is then very interesting to understand the robustness of QSH states in III-V-monolayer/SiO_2 and further elaborate on the role of p_z.

To this end, we study the magnetic response under both a longitudinal and transversal field. We simulate the developments of the Landau levels (LLs) under a perpendicular magnetic field B_z by introducing a Peierls phase in the model Hamiltonian of the nanoribbon. As shown in Figs. 2(b), 2(e) and 2(h), with the increase of B_z, the bulk LLs of the conduction/valence bands hardly change, and they do not cross under any experimentally accessible strength of the magnetic field. Thus, owing to the large topological gap the bulk band topology is much more robust than in HgTe and InAs/GaSb. One cannot destroy the QSH states by only breaking the time-reversal symmetry in III-V-monolayer/SiO_2.

However, the edge states can be gapped in the presence of the p_z orbital and the breaking of inversion symmetry. Note that, under a perpendicular magnetic field, B_z mixes opposite helicities. Edge states are not severely destroyed and they may persist nearly gapless, as exemplified by the inversion-symmetric HgTe quantum wells [41–52]. We find that, for III-V films with broken inversion symmetry, the gaps of the topological edge states are always negligibly small although the Rashba band splitting is fairly large. The six subplots on the right-hand side of Fig. 2 are zoomed-in plots of edge Dirac points denoted by the red arrows in Figs. 2(c), 2(f) and 2(i) under B_x and B_z, correspondingly. With all three p orbitals as shown in Fig. 2(c), the edge states are gapped under both in-plane and out-of-plane magnetic fields, but only in the order of meV, while, with vanishing SOC coupling between $p_{x/y}$ and p_z [Fig. 2(f)] or with only $p_{x/y}$ orbitals [Fig. 2(i)], the edge Dirac points in this inversion-asymmetric environment remain gapless under B_z. Going from the simplified model to the full DFT band structure, after taking into account all sublattice asymmetry and the substrate effect, we find the gap on the edge states induced by the external magnetic field and the breaking of inversion symmetry remains tiny in both systems. The largest gap resolved in our calculations is only 1.4 meV under $B_z = 10$ T, as shown in Fig. 3. Bonding of p_z with β-SiO_2 leads to an even smaller gap between the edges states under B_z. Thus, a conductance measurement of the III-V-monolayer/SiO_2 may observe a more robust quantized plateau (in a large range of experimentally accessible magnetic fields B_z) than in HgTe, which is highly promising for device application.

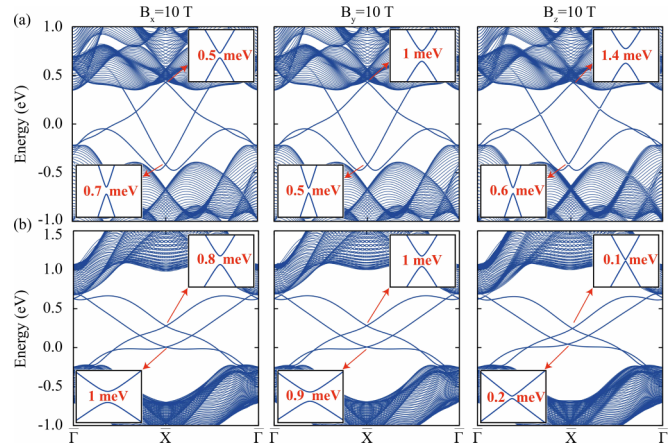

FIG. 3. Magnetic responses of III-V-monolayer/SiO_2. (a) TlBi/α-SiO_2. (b) TlBi/β-SiO_2. The insets are zoomed-in plots in an energy range of 5 meV and a k range of 0.05/Å.

V. CONCLUSION

We have designed a universal band inversion model Hamiltonian which applies to planar/buckled hexagonal sheets of p orbitals. Based on our model, the QSH state readily emerges from gapping the degenerate bonding/antibonding states of $p_{x,y}$. The off-diagonal SOC sector, which hybridizes opposite spins and sublattice degrees of freedom, is of crucial importance. On the one hand, it reduces the topological gap sizes via Rashba splitting, and on the other hand, opens gaps on edge states in perpendicular magnetic fields. These two effects manifest themselves in realistic systems and offer us a tuning parameter to guide the engineering of promising, application-relevant QSH platforms.

Our analysis offers two strategies to boost topological gaps through the manipulation of p_z orbitals. One is to change the QSHE formation mechanism from Kane-Mele type to band inversion type, such that the Rashba band splitting is significantly reduced at Γ as exemplified in α-quartz SiO_2. The other is to directly bond p_z orbitals, e.g., those of the III-V monolayer, to β-tridymite SiO_2. This eliminates the aforementioned off-diagonal couplings, and promotes the topological gap up to scales of 907 meV in TlBi, taking full advantage of the $p_{x/y}$ intrinsic SOC. We also note that Kane-Mele and band inversion mechanisms are two phenomenological criteria that help to quickly justify the QSH phase. They are essentially the same in terms of Berry curvature change [53] and elementary band representation splitting [54].

The implementation of the band inversion type topological mechanism in two-dimensional III-V monolayers, together with our proposed tight-binding model universality class, generically applies to all p hexagonal monolayers, providing a platform for possible future in-depth theoretical and experimental studies. The large-gap QSH edge states in the III-V-monolayer/SiO_2 systems appear highly promising for room-temperature fabrication and manipulation. We hope that our work thus lays out a path to elevate QSH from a low-temperature quantum phenomenon to an implementable effect in modern electronic devices.

Note added. The very recent preprint by Shenglong Xu and Congjun Wu [55] came to our attention at the proof stage of our paper. These authors reveal a quadratic band touching between the $p_x - p_y$ orbitals at the Γ point by using a symmetry principle. This is consistent with our findings in material calculations.

ACKNOWLEDGMENTS

This work was supported by the National Key R&D Program of China (Grant No. 2017YFE0131300), Sino-German Mobility Program No. M-0006, National Natural Science Foundation of China under Grant No. 11874263, and Shanghai Technology Innovation Action Plan 2020–Integrated Circuit Technology Support Program (Project No. 20DZ1100605). This work in Würzburg is funded by the Deutsche Forschungsgemeinschaft (DFG, German Research Foundation) through Project-ID 258499086 - SFB 1170 and through the Würzburg-Dresden Cluster of Excellence on Complexity and Topology in Quantum Matter - ct.qmat Project-ID 390858490 - EXC 2147. Calculations were carried out at the HPC Platform of ShanghaiTech Laboratory for Topological Physics and School of Physical Science and Technology.

[1] C. L. Kane and E. J. Mele, Phys. Rev. Lett. **95**, 226801 (2005).
[2] C. L. Kane and E. J. Mele, Phys. Rev. Lett. **95**, 146802 (2005).
[3] B. A. Bernevig, T. L. Hughes, and S.-C. Zhang, Science **314**, 1757 (2006).
[4] M. König, S. Wiedmann1, C. Brüne1, A. Roth, H. Buhmann, L. W. Molenkamp, X.-L. Qi, and S.-C. Zhang, Science **318**, 766 (2007).
[5] C.-C. Liu, W. Feng, and Y. Yao, Phys. Rev. Lett. **107**, 076802 (2011).
[6] Y. Xu, B. Yan, H.-J. Zhang, J. Wang, G. Xu, P. Tang, W. Duan, and S.-C. Zhang, Phys. Rev. Lett. **111**, 136804 (2013).
[7] Z. Liu, C.-X. Liu, Y.-S. Wu, W.-H. Duan, F. Liu, and J. Wu, Phys. Rev. Lett. **107**, 136805 (2011).
[8] M. Wada, S. Murakami, F. Freimuth, and G. Bihlmayer, Phys. Rev. B **83**, 121310(R) (2011).
[9] S. Murakami, Phys. Rev. Lett. **97**, 236805 (2006).
[10] F. Reis, G. Li, L. Dudy, M. Bauernfeind, S. Glass, W. Hanke, R. Thomale, J. Schäfer, and R. Claessen, Science **357**, 287 (2017).
[11] G. Li, W. Hanke, E. M. Hankiewicz, F. Reis, J. Schäfer, R. Claessen, C. Wu, and R. Thomale, Phys. Rev. B **98**, 165146 (2018).
[12] S. Glass, F. Reis, M. Bauernfeind, J. Aulbach, M. R. Scholz, F. Adler, L. Dudy, G. Li, R. Claessen, and J. Schäfer, J. Phys. Chem. C **120**, 10361 (2016).
[13] F.-C. Chuang, L.-Z. Yao, Z.-Q. Huang, Y.-T. Liu, C.-H. Hsu, T. Das, H. Lin, and A. Bansil, Nano Lett. **14**, 2505 (2014).
[14] X. Li, Y. Dai, Y. Ma, W. Wei, L. Yu, and B. Huang, Nano Res. **8**, 2954 (2015).
[15] C. P. Crisostomo, L.-Z. Yao, Z.-Q. Huang, C.-H. Hsu, F.-C. Chuang, H. Lin, M. A. Albao, and A. Bansil, Nano Lett. **15**, 6568 (2015).
[16] Y. Ma, X. Li, L. Kou, B. Yan, C. Niu, Y. Dai, and T. Heine, Phys. Rev. B **91**, 235306 (2015).
[17] Y. Zhang, H. Ye, Z. Yu, H. Gao, and Y. Liu, RSC Adv. **8**, 7022 (2018).
[18] Y. Kim, W. S. Yun, and J. D. Lee, Sci. Rep. **6**, 33395 (2016).
[19] R. R. Q. Freitas, R. Rivelino, F. de Brito Mota, C. M. C. de Castilho, A. Kakanakova-Georgieva, and G. K. Gueorguiev, J. Phys. Chem. C **119**, 23599 (2015).
[20] M. Barhoumi, K. Lazaar, and M. Said, J. Fluorine Chem. **212**, 171 (2018).
[21] L. Li, X. Zhang, X. Chen, and M. Zhao, Nano Lett. **15**, 1296 (2015).
[22] R. R. Q. Freitas, F. de Brito Mota, R. Rivelino, C. M. C. de Castilho, A. Kakanakova-Georgieva, and G. K. Gueorguiev, Nanotechnology **27**, 055704 (2016).
[23] S.-s. Li, W.-x. Ji, C.-w. Zhang, S.-j. Hu, P. Li, P.-j. Wang, B.-m. Zhang, and C.-l. Cao, Sci. Rep. **6**, 23242 (2016).
[24] Q. Lu, B. Wang, X.-R. Chen, and W.-M. Liu, Phys. Rev. Mater. **2**, 014005 (2018).
[25] Q. Lu, R. Ran, Y. Cheng, B. Wang, Z.-Y. Zeng, and X.-R. Chen, J. Appl. Phys. **124**, 035305 (2018).
[26] J. E. Padilha, A. Janotti, A. Fazzio, and A. J. R. da Silva, Phys. Rev. B **94**, 195424 (2016).
[27] L.-Z. Yao, C. P. Crisostomo, C.-C. Yeh, S.-M. Lai, Z.-Q. Huang, C.-H. Hsu, F.-C. Chuang, H. Lin, and A. Bansil, Sci. Rep. **5**, 15463 (2015).
[28] N. Denisov, A. Alekseev, O. Utas, S. Azatyan, A. Zotov, and A. Saranin, Surf. Sci. **651**, 105 (2016).
[29] C.-H. Hsu, Z.-Q. Huang, C.-Y. Lin, G. M. Macam, Y.-Z. Huang, D.-S. Lin, T. C. Chiang, H. Lin, F.-C. Chuang, and L. Huang, Phys. Rev. B **98**, 121404(R) (2018).
[30] See Supplemental Material at http://link.aps.org/supplemental/10.1103/PhysRevB.106.165203 for details of the crystal structure and the electronic and topological analysis, which includes Refs. [31–36].
[31] G. Kresse and J. Furthmüller, Phys. Rev. B **54**, 11169 (1996).
[32] J. P. Perdew, K. Burke, and M. Ernzerhof, Phys. Rev. Lett. **77**, 3865 (1996).
[33] N. Marzari and D. Vanderbilt, Phys. Rev. B **56**, 12847 (1997).
[34] A. A. Mostofi, J. R. Yates, Y.-S. Lee, I. Souza, D. Vanderbilt, and N. Marzari, Comput. Phys. Commun. **178**, 685 (2008).
[35] M. P. L. Sancho, J. M. L. Sancho, and J. Rubio, J. Phys. F: Met. Phys. **15**, 851 (1985).
[36] M. Nakhaee, S. A. Ketabi, and F. M. Peeters, Comput. Phys. Commun. **254**, 107379 (2020).
[37] H. d'Amour, W. Denner, and H. Schulz, Acta Crystallogr., Sect. B: Struct. Sci. **35**, 550 (1979).
[38] V. Presser and K. G. Nickel, Crit. Rev. Solid State Mater. Sci. **33**, 1 (2008).

[39] J. C. Slater and G. F. Koster, Phys. Rev. **94**, 1498 (1954).
[40] L. Du, I. Knez, G. Sullivan, and R.-R. Du, Phys. Rev. Lett. **114**, 096802 (2015).
[41] S.-B. Zhang, Y.-Y. Zhang, and S.-Q. Shen, Phys. Rev. B **90**, 115305 (2014).
[42] J. Maciejko, X.-L. Qi, and S.-C. Zhang, Phys. Rev. B **82**, 155310 (2010).
[43] W. Beugeling, N. Goldman, and C. M. Smith, Phys. Rev. B **86**, 075118 (2012).
[44] F. Dominguez, B. Scharf, G. Li, J. Schäfer, R. Claessen, W. Hanke, R. Thomale, and E. M. Hankiewicz, Phys. Rev. B **98**, 161407(R) (2018).
[45] D. G. Rothe, R. W. Reinthaler, C.-X. Liu, L. W. Molenkamp, S.-C. Zhang, and E. M. Hankiewicz, New J. Phys. **12**, 065012 (2010).
[46] R. Ilan, J. Cayssol, J. H. Bardarson, and J. E. Moore, Phys. Rev. Lett. **109**, 216602 (2012).
[47] J.-c. Chen, J. Wang, and Q.-f. Sun, Phys. Rev. B **85**, 125401 (2012).
[48] B. Scharf, A. Matos-Abiague, and J. Fabian, Phys. Rev. B **86**, 075418 (2012).
[49] B. Scharf, A. Matos-Abiague, I. Žutić, and J. Fabian, Phys. Rev. B **91**, 235433 (2015).
[50] M. Kharitonov, S. Juergens, and B. Trauzettel, Phys. Rev. B **94**, 035146 (2016).
[51] G. Tkachov and E. M. Hankiewicz, Phys. Rev. Lett. **104**, 166803 (2010).
[52] G. Tkachov and E. Hankiewicz, Phys. E **44**, 900 (2012).
[53] W.-x. Ji, C.-w. Zhang, M. Ding, B.-m. Zhang, P. Li, F. Li, M.-j. Ren, P.-j. Wang, R.-w. Zhang, S.-j. Hu, and S.-s. Yan, New J. Phys. **18**, 083002 (2016).
[54] J. Deng, D. Shao, J. Gao, C. Yue, H. Weng, Z. Fang, and Z. Wang, Phys. Rev. B **105**, 224103 (2022).
[55] S. Xu and C. Wu, arXiv:2209.14510v1.